Published in final edited form as:
Ann Biomed Eng. 2009 May ; 37(5): 902–912. doi:10.1007/s10439-009-9665-6.

Application of L1-Norm Regularization to Epicardial Potential Solution of the Inverse Electrocardiography Problem

Subham Ghosh and **Yoram Rudy**
Cardiac Bioelectricity and Arrhythmia Center (CBAC) and Department of Biomedical Engineering, Washington University in St Louis, St Louis, Missouri 63130

Abstract

The electrocardiographic inverse problem of computing epicardial potentials from multi-electrode body-surface ECG measurements, is an ill-posed problem. Tikhonov regularization is commonly employed, which imposes penalty on the L2-norm of the potentials (zero-order) or their derivatives. Previous work has indicated superior results using L2-norm of the normal derivative of the solution (a first order regularization). However, L2-norm penalty function can cause considerable smoothing of the solution. Here, we use the L1-norm of the normal derivative of the potential as a penalty function. L1-norm solutions were compared to zero-order and first-order L2-norm Tikhonov solutions and to measured gold standards in previous experiments with isolated canine hearts. Solutions with L1-norm penalty function (average relative error [RE] = 0.36) were more accurate than L2-norm (average RE= 0.62). In addition, the L1-norm method localized epicardial pacing sites with better accuracy (3.8±1.5 mm) compared to L2-norm (9.2±2.6 mm) during pacing in five pediatric patients with congenital heart disease. In a pediatric patient with Wolff-Parkinson-White syndrome, the L1-norm method also detected and localized two distinct areas of early activation around the mitral valve annulus, indicating the presence of two left-sided pathways which were not distinguished using L2 regularization.

Keywords

Electrocardiographic inverse problem; Tikhonov regularization; Total variation regularization

INTRODUCTION

Electrocardiographic Imaging (ECGI)[27] is an imaging modality for noninvasive mapping of cardiac electrical activity in humans. It reconstructs epicardial potentials, electrograms, activation (isochrones) and recovery sequences on the epicardial surface of the heart from 250 body- surface electrocardiograms (ECG) and an ECG-gated thoracic CT scan. The theoretical basis for ECGI is a potential-based inverse problem[29] for Laplace s equation. Martin and Pilkington[23] were among the first to study the relationship between epicardial and body-surface potentials using simple geometry. Barr and Spach[3] and Colli-Franzone et al[8] have made early seminal contributions to the methodology of solving the electrocardiographic inverse problem. The inverse solution in terms of epicardial potentials is unique and epicardial potentials have been shown to reflect underlying myocardial activity[30]. Recently, ECGI has been applied in the clinical setting[15,16,19,20,35,36] after extensive validation in animal studies[5,6,24,26].

Address correspondence to: Yoram Rudy, Director, Cardiac Bioelectricity Center, 290 Whitaker Hall, Campus Box 1097, One Brookings Dr., Saint Louis, Missouri, 63130-4899, Tel : (314) 935-8160 Fax : (314) 935-8168, rudy@wustl.edu, URL: http://rudylab.wustl.edu.

Alternative approaches to the inverse problem include representation of cardiac electrical activity by several fixed or moving dipoles[8] and model-based activation imaging which aims at reconstructing the activation sequence on both endocardial and epicardial surfaces[9,32] or over the myocardial volume.[38] While activation imaging yields a unique solution and has been shown[7] to be less affected by measurement noise than the potential-based method, it does not provide information about the entire cardiac cycle which includes both activation and repolarization. Another approach, alternative to the potential-based method, is imaging of cardiac transmembrane potentials, a concept that stemmed from the work of Geselowitz and Miller[13] and later developed and implemented by Fischer et al[12].

ECGI was validated extensively in canine-heart experiments during normal sinus rhythm[24] and ventricular pacing[26]. It was used to image electrophysiologic substrate and reentrant ventricular tachycardia in infarcted hearts[5,6]. It was also shown to image cardiac repolarization and its spatial dispersion[14]. ECGI was applied to image cardiac excitation in humans under normal[27,28] as well as a variety of pathophysiological conditions[15,16,19,20,35,36]. Recently, ECGI was applied successfully in the pediatric population[15,16], though with smaller number of electrodes (160–200) due to smaller torso-size.

The procedure of ECGI involves solving Laplace s equation in the source-free volume conductor between the epicardial and torso surfaces. Boundary Element Method (BEM)[4] is applied to discretize the torso and the epicardial surfaces to derive a relationship between the epicardial potentials ($\mathbf{V_E}$) and the torso potentials ($\mathbf{V_T}$) : $\mathbf{AV_E = V_T}$. The transfer matrix **A** is derived by solving the boundary integral formulation of Laplace s equation for the well-posed forward problem using the boundary element method. The boundary in this particular problem consists of the epicardial surface of the heart and the torso surface defined by the position of the torso-electrodes. The surface geometries (coordinates) are obtained by accurate measurement with a digitizer in the case of canine experiments and from ECG-gated CT scans in the case of human studies. Thus the matrix **A** represents the heart-torso geometrical relationship. It does not depend on a stylized model of the heart-torso, rather it is specific to each study subject (human or canine).

The transfer matrix A is ill-posed and $\mathbf{V_E}$ is computed from $\mathbf{V_T}$ using Tikhonov regularization[31] where the objective function is

$$\min_{\mathbf{V_E}}\{\left\|\mathbf{V_T} - \mathbf{AV_E}\right\|_2^2 + \lambda^2\left\|\mathbf{FV_E}\right\|_2^2\}$$

In the above expression, the first term is the least square minimization term while the second term places a penalty or constraint on the L2-norm of the solution or its derivatives, depending on the operator **F**. λ is the regularization parameter, chosen by the L-curve or other methods[18,29]. **F** is an operator which is usually taken as the identity matrix, thereby placing a constraint on the amplitude of the reconstructed epicardial potentials (zero-order Tikhonov [ZOT]). Choice of the penalty function affects the solution. Previous work[22,33] has indicated superior results obtained by using the L2-norm of the normal derivative of the potential ($\partial\mathbf{V_E}/\partial\mathbf{n}$) as a penalty function, a first order Tikhonov (FOT) scheme. However, use of a L2-norm based penalty has a spatial smoothing effect on the solution which may lead to the loss of diagnostically meaningful information (e.g. accurately localizing an arrhythmic focus or resolving two distinct foci in close spatial proximity). Various regularization algorithms have been applied to the ECG inverse problem, mostly based on Tikhonov regularization that imposes L2-norm constraints. Ahmad et al[1] introduced the possibility of imposing multiple constraints for improving the ECG inverse solution. Spatiotemporal regularization methods have been also developed by different groups[17,25] working on this problem. However, these

L2-based algorithms smooth the solution, which may reduce the accuracy of localizing cardiac sources and of resolving multiple sources in close spatial proximity.

Non-quadratic regularization technique, alternatively known as total-variation regularization[11,21,34], has been applied with considerable success in the field of image restoration, especially in restoring high-frequency spatial features of the image. A rich body of literature[2,10,37] also exists on the development of L1 norm approaches for bioelectric source imaging problems in the field of magnetoencephalography (MEG) and electroencephalography (EEG). Wolters et al[37] developed an L1-norm approach for source reconstruction problems in MEG. The L1-norm approach has been also developed for sparse source imaging[10] in EEG. Bai et al[2] have established the L1-norm method as superior to higher order norms for cortical current density imaging with realistic anatomic models derived from patients undergoing neurosurgical evaluation. This technique penalizes the L1-norm of the gradient function and yields less-smoothed solutions with more localized details. There have been no previous studies involving application of non-quadratic regularization in the electrocardiographic inverse problem. Here, we apply a regularization scheme based on penalizing the L1-norm of the normal derivative of the potential. We compare the solutions of this scheme with L2-norm based Tikhonov regularization in different experimental preparations of canine hearts, as well as in clinical applications in pediatric patients.

METHODS

Computational Methods

The objective function using an L1-norm based penalty is given by

$$T(\mathbf{V_E}) = \left\|\mathbf{AV_E} - \mathbf{V_T}\right\|_2 + \lambda^2 \left\|\partial \mathbf{V_E}/\partial \mathbf{n}\right\|_1 \quad (1)$$

where λ is the regularization parameter chosen by the L-curve technique[18] and the subscripts 1 and 2 indicate L1 and L2 norms respectively. Logarithmic plots (base 10) of the L1 norm of the solution s normal derivative versus the residual L2-norm are L-shaped for all datasets and are amenable to L-curve analysis commonly performed in Tikhonov regularization for choosing a regularization parameter. L-curve plots are shown in Figure 1 for three different datasets: single site pacing (left), post-infarct canine data (middle) and the data for the WPW patient (right).

A BEM solution of Laplace s equation, applied to the torso and epicardial surfaces comprising the boundaries, yields the following matrix equations [4]

$$\begin{aligned} \mathbf{C} * [\ \mathbf{V_T}\ \ \partial \mathbf{V_E}/\partial \mathbf{n}\ ]^{\mathbf{t}} &= \mathbf{B} * [\ \mathbf{0}\ \ \mathbf{V_E}\ ]^{\mathbf{t}} \\ [\ \mathbf{V_T}\ \ \partial \mathbf{V_E}/\partial \mathbf{n}\ ]^{\mathbf{t}} &= [\mathbf{C^{-1}B}] * [\ \mathbf{0}\ \ \mathbf{V_E}\ ]^{\mathbf{t}} \end{aligned} \quad (2)$$

The equation (2) above is derived by reordering the set of equations which relate the potential (**V**) and its normal derivative (***∂*V/*∂*n**) at each boundary node. These equations are obtained by formulation of the boundary integral equation for Laplace s problem, using the fundamental solution (Green s function) as a weighting function[4]. The reordering is performed in such a way that potential at the torso boundary, $\mathbf{V_T}$ and the normal derivative of the potential at the epicardial boundary, $\partial \mathbf{V_E} / \partial \mathbf{n}$ are on the left side while $\partial \mathbf{V_T} / \partial \mathbf{n}$ and $\mathbf{V_E}$ are on the right side. (Note that if the subject is in non-conductive air, $\partial \mathbf{V_T} / \partial \mathbf{n} = \mathbf{0}$). B and C are the BEM transfer matrices[4].

By extracting the appropriate rows and columns of the matrix $\mathbf{C^{-1}B}$, a transfer matrix $\mathbf{D}$ can be derived relating $\partial \mathbf{V_E} / \partial \mathbf{n}$ to $\mathbf{V_E}$:

$$[\partial \mathbf{V}_E / \partial \mathbf{n}] = \mathbf{D}[\mathbf{V}_E] \tag{3}$$

Thus the objective function can be expressed as

$$T(\mathbf{V}_E) = \left\| \mathbf{A}\mathbf{V}_E - \mathbf{V}_T \right\|_2 + \lambda^2 \left\| \mathbf{D}\mathbf{V}_E \right\|_1 \tag{4}$$

The above formulation leads to a non-linear optimization problem due to non-differentiability of the L1-norm penalty function. It has been shown[21] that an estimate of the solution can be obtained by solving the following set of equations as $\beta \rightarrow 0$.

$$(\mathbf{A}^t\mathbf{A} + \lambda^2 \mathbf{D}^t \mathbf{W}_{\beta}(\mathbf{V}_E)\, \mathbf{D})\, \mathbf{V}_E = \mathbf{A}^t \mathbf{V}_T \tag{5}$$

where the diagonal weight matrix $\mathbf{W_\beta}$ is obtained by

$$\mathbf{W}_{\beta}(\mathbf{V}_E) = 1/2\ \mathrm{diag}[\,1/\sqrt{(|[\mathbf{D}\mathbf{V}_E]_i|^2 + \beta)}], \tag{6}$$

and β is a small positive constant. For each dataset presented here, β is assigned a value of 10^{-5} and is kept fixed at this value for all iterations. The L1-norm of the derivative is approximated as $\preccurlyeq \mathbf{D}\mathbf{V_E} \preccurlyeq_{i=1} \Sigma^n \sqrt{(\preccurlyeq [\mathbf{D}\mathbf{V_E}]_i \preccurlyeq^2 + \beta)}$. Thus when the local derivative is small, the weight goes to a large value imposing greater smoothness on the solution. When the local derivative is large, the weight goes to a small value, allowing large gradients in solution coefficients at these locations. This leads to correct estimation of gradients, as opposed to L2-norm based constraints which may overestimate or underestimate the solution gradients depending on the penalty function.

Computationally, the equation is still non-linear since the weight matrix depends on the solution $\mathbf{V_E}$. However, it can be estimated by a fixed point iteration for $\mathbf{V_E}$, only requiring the solution of a standard linear problem at each step. Thus

$$(\mathbf{A}^t\mathbf{A} + \lambda^2 \mathbf{D}^t \mathbf{W}_{\beta}(\mathbf{V}_E^{\,k})\mathbf{D})\, \mathbf{V}_E^{\,k+1} = \mathbf{A}^t \mathbf{V}_T \tag{7}$$

where $\mathbf{V_E^k}$ is the solution at the kth iteration, starting with an initial guess of zero. The computing time may be reduced by setting the starting guess at the j-th time step of the cardiac cycle to the fixed iterative solution obtained at the (j-1)-th time step, since the solution can be assumed to be a continuous function of time at high sampling rates (≥ 1 KHz).

Experimental Methods and Protocols

We evaluated and compared the L1 norm regularized solutions to those of L2 norm-based Tikhonov solutions using data from previously performed experiments in isolated canine hearts[6,14,26]. In addition, we compared the accuracy of localization of epicardial pacing sites by these methods in five pediatric patients undergoing cardiac resynchronization therapy, using

the CT coordinates of the tip of the pacing lead as the gold standard. Lastly, we present a single example of a pediatric WPW patient[15] where we used the two methods to localize the pre-excitation area noninvasively to guide intracardiac catheter mapping and ablation. The sampling rate for canine and human data presented here are 1 and 2 KHz, respectively. A brief description of the protocols is provided below :

a. *Pacing of an Isolated Canine Heart in a Human-shaped Torso Tank*[26] : This set up consisted of an isolated canine heart suspended in a homogenous electrolytic medium in the correct anatomical position inside a tank molded in the shape of a human torso. The tank had 384 surface electrodes recording torso potentials and 242 rods with electrodes at their tips that formed an epicardial recording envelope around the heart. The torso-surface potentials and epicardial potentials were recorded simultaneously. The torso-surface potentials provided the input data for ECGI reconstruction of epicardial potentials, electrograms and isochrones which were then evaluated by comparison with those measured directly by the rod-tip electrodes. Data obtained during epicardial pacing from an anterior right ventricular (RV) site were used.

b. *Infarct Substrate*[6]: Epicardial potentials during right atrial (RA) pacing (simulating normal sinus rhythm) were recorded from a 490-electrode sock. A region of infarcted tissue was created in the left ventricle (LV) by ligation of the left anterior descending coronary artery (LAD) and ethanol injection. Details of the experiment are provided in the original publication[6]. The measured epicardial potentials were used to compute body-surface potentials in a homogeneous computer model of the human torso. Measurement noise (100 μV peak to peak, Gaussian) and geometrical errors 5 mm Gaussian) were added to the body-surface potentials and the electrode positions respectively, to simulate experimental or clinical measurements. These data were used to reconstruct epicardial potentials by ZOT and FOT as well as the L1-norm based regularization schemes.

c. *Dispersion of Repolarization*[14]: Abnormal and heterogeneous repolarization provides a substrate for reentrant arrhythmias. In this experiment localized cooling and warming of adjacent regions in the LV epicardium was performed to induce high spatial dispersion of repolarization. Epicardial potentials were recorded during RA pacing and QRST integral maps were computed to reflect local repolarization properties. Realistic body-surface potentials were then generated from these measurements using the same methods as described in b). These were used to perform the ECGI reconstructions and compute reconstructed epicardial QRST integral maps.

d. Pacing in Pediatric CRT Patients : ECGI was performed during pacing from epicardial sites in five pediatric heart failure patients with congenital heart disease, who are undergoing CRT. Due to the smaller torso size of pediatric patients, 160–192 electrodes were applied to the body surface instead of the usual 250 electrodes for ECGI in adults. 160 body-surface electrodes were applied for children less than 12 years old. 192 torso-electrodes were applied for patients aged between 12–18 years. A pacing site simulates an ectopic focus and these data were used to ascertain the relative localization accuracy of the L1 and L2 norm-based methods for patients with smaller torso size and reduced number of body-surface electrodes.

e. Pediatric Wolff-Parkinson-White (WPW) Patient : We compared the L1 and L2 norm reconstructed ECGI activation maps in a pediatric patient with WPW syndrome to noninvasively locate the region of pre-excitation and guide intracardiac mapping and ablation. These data demonstrated the clinical utility of the L1 norm method in producing higher resolution activation-maps compared to the L2 norm.

Data Processing and Evaluation Protocol

For datasets obtained from experiments with isolated canine hearts, L1-norm and L2-norm ZOT/FOT reconstructions were compared to directly measured epicardial data, which served as the gold standard. A zero initial value was used as a starting point for the fixed iterations for obtaining the L1-norm solutions. The regularization parameter λ was chosen by the L-curve method. Typically, two quantities were reconstructed : a) epicardial potential maps which depicted the spatial distribution of voltage on the epicardial surface at a given time instant during the cardiac cycle b) electrograms which depicted the variation of voltage as a function of time at a given point on the epicardial space. In addition, epicardial QRST integral maps were constructed for depicting local repolarization properties for the dataset on dispersion of repolarization in isolated canine heart. Quantitative measures of ECGI accuracy were obtained by computing relative errors (RE) and correlation coefficients (CC) between the reconstructed and measured epicardial data.

$$RE=\sqrt{[\sum_{i=1}^{N}(Vi^{C}-V_i^{M})^2/\sum_{i=1}^{N}(V_i^{M})^2]} \tag{8}$$

$$CC=\sum_{i=1}^{N}(V_i^{M}-V_m^{M})(V_i^{C}-V_m^{C})/\sqrt{[\sum_{i=1}^{N}(V_i^{M}-V_m^{M})^2\sum_{i=1}^{N}(V_i^{C}-V_m^{C})^2]} \tag{9}$$

where N is the number of epicardial nodes for comparing epicardial potentials or number of time-points for comparing electrograms. V_i^C is the noninvasively reconstructed (computed) epicardial data at the i^{th} node or time-point, V_i^M is the corresponding measured data, V_m^C and V_m^M are their respective mean values. For epicardial potential maps, RE gives a measure of overall accuracy of the reconstructions while CC indicates how well the spatial pattern of reconstructed potentials is preserved with respect to the measured data. Representative values of RE and CC are averaged over the entire cardiac cycle. For electrograms, CC indicates how well the reconstructed electrogram resembles the measured electrogram in morphology.

L1-norm and FOT L2-norm regularization methods were used for computation of ECGI data in humans. For the datasets on pacing in pediatric heart failure patients, accuracy of localization of pacing sites from the reconstructed spatial epicardial potential maps was computed with respect to the CT coordinates of the tip of the epicardial pacing lead. The pacing site was localized from the computed epicardial potential maps at the geometrical center of the quasi-elliptic region of negative potentials that develops on the epicardial surface during the initial phase (10–20 ms) of activation during paced rhythm. (The geometric center of a collection of n points with Cartesian coordinates **x** is defined as $\Sigma\mathbf{x}/n$). The overall accuracy of localization, taken over all the subjects, is expressed as mean ± standard deviation. ECGI data from the pediatric WPW patient is presented in the form of epicardial activation-isochrones. Activation-isochrone map is computed from the reconstructed epicardial electrograms by assigning local activation time as the time-point when the negative time derivative of the electrogram reached a maximum($-dV/dt_{max}$). Areas of early activation in the pre-excited rhythm identified sites of pre-excitation in the WPW patient. ECGI data in the human subjects were also compared visually for qualitative assessment of the solutions obtained from the two methods.

RESULTS

Pacing of an Isolated Canine Heart in a Human-shaped Torso Tank

Figure 2 shows the epicardial potential maps during pacing, 15 ms after onset of QRS. Panel A shows the measured data, with the pacing site marked by an asterisk. A quasi-elliptic area of negative potential (dark blue) develops around the pacing site, flanked by areas of positive potentials (red). L2-ZOT reconstructed data are shown in panel B. While ZOT reconstructs the pattern of negative potentials (dark blue) around the pacing site (asterisk) flanked by a region of positive potentials (red), it overestimates the spatial gradients between the area of negative potentials and the area of positive potentials on the flanks, leading to significant errors in the reconstruction (RE = 1.40 and CC=0.79). Panel C shows the L2-norm FOT solution. Though the overall accuracy of reconstruction improves (RE = 0.82, CC= 0.81), the solution is overly smoothed. Panel D shows the L1-norm reconstructions. L1-norm solution not only preserves the shape of the region of negative voltage (dark blue) but also provides a more accurate estimate of the spatial voltage gradients (blue to red) around the pacing site, resulting in improvement in overall accuracy (RE =0.61) and preservation of spatial features (CC=0.89).

Infarct Substrate

The first row in figure 3 shows the measured (panel A), L2-ZOT (panel B), L2-FOT (panel C) and L1-norm reconstructed epicardial potentials (panel D) *pre- infarct*, 45 ms after onset of QRS during activation. The second row (panels E-H) shows the corresponding data *post-infarct*. Both pre-infarct and post-infarct, epicardial potential levels as well the spatial voltage gradients are most accurately reflected in the L1-norm constrained reconstructions (RE=0.72, CC = 0.91 [pre], RE=0.23, CC=0.96 [post]) compared to ZOT (RE=0.85, CC=0.87 [pre], RE=0.32, CC=0.93 [post]) and FOT (RE=0.75, CC=0.86 [pre], RE=0.28, CC=0.91[post]). The localized potential minimum (dark blue, panel E) to the immediate right of the left anterior descending coronary artery (LAD) in the post-infarct measured data is smoothed out in the L2 norm reconstructions (panels F and G). Figure 4 shows the epicardial electrograms pre-and post infarction. Electrograms are displayed from three epicardial sites marked in the cartoon of the heart in panel A. Rows 1 and 2 show the pre-(top) and post-infarct (bottom) electrograms from LV sites 1 and 2 within the infarct area marked in panel A. Row 3 shows electrograms (pre-infarct, top; post-infarct bottom) from a RV site 3 remote to the infarct area. While morphology of the electrogram at site 3 remains unchanged, electrograms at sites 1 and 2 become negative and fractionated post-infarct with multiple deflections. The L1-norm scheme preserves better than L2 the multiple deflections and morphologies of the post-infarct electrograms (CC= 0.97 compared to 0.87 for ZOT and 0.86 for FOT).

Dispersion of Repolarization

Epicardial QRST integral maps computed from measured and reconstructed epicardial data during simultaneous LV warming and cooling are shown in Figure 5. High QRST integral values (in red, panel A) are observed in the warmed area of the LV while lower values (dark blue, panel A) are obtained in the adjacent cooler regions, reflecting heterogeneous repolarization. The reconstructed maps (panels B-D) capture the areas of low (dark blue) and high (red, orange) QRST integral values. The FOT (panel C) and the L1-norm (panel D) QRST integral maps show similar correlation values of 0.96 and 0.94 respectively to the measured data. ZOT QRST integral map (panel B) has a lower correlation (0.87) and erroneously shows a sharp QRST gradient (orange to dark blue) in the superior part of the ventricle to the right of LAD.

Pacing in Pediatric CRT Patients

Figure 6 shows ECGI epicardial potential maps during early activation (10–20 ms after onset of QRS in the paced rhythm) in pediatric CRT patients with congenital heart disease. The first two panels in each row show the right anterior oblique (RAO) view during pacing from a right-sided or a posterior lead alone. The third and fourth panels in each row show the left lateral (LL) view during pacing from the left-sided or anterior lead alone. The top row shows the epicardial potential map in a 6 year old female patient with congenital heart block, undergoing CRT. She had two epicardial pacing leads surgically implanted, one in the RV apex and the other in the LV lateral wall. The positions of the tip of the pacing leads, determined from CT, are marked by white asterisks. Panels A and B show epicardial potential map 15 ms after onset of QRS during pacing from the RV lead alone. The FOT solution (panel A) shows a large smoothed out area of negative potentials (dark blue) while the L1 norm (panel B) shows a more localized (dark blue) area of negative potentials around the pacing site. The accuracy of localization of the RV pacing site with respect to the CT location of the lead is 10 mm (FOT) and 2 mm (L1 norm). Panels C and D show the ECGI epicardial potential maps 18 ms after onset of QRS during pacing from the LV lead alone. The localization error of the LV pacing site is 14 mm (FOT, panel C) and 6 mm (L1 norm). Figure 5, second row shows comparison of localization of pacing sites in a 5 year-old male patient with corrected congenital transposition of the great arteries (cc TGA) and congenital heart block, also undergoing CRT with epicardial leads. Errors of localization of the pacing leads from the ECGI potential maps are 7 mm (FOT, panel E) and 4 mm (L1 norm, panel F) for the pulmonary ventricle lead and 12 mm (FOT, panel G) and 6 mm (L1 norm, panel H) for the systemic ventricle lead. Figure 5, third row shows the ECGI reconstructed potential maps during pacing from posterior (RAO view, panels I and J) and anterior leads (LL view, panels K and L) in a 17 year old female patient with a single double inlet left ventricle (status-post [s/p] Fontan) and congenital atrioventricular (AV) node block. Her posterior lead is localized from the ECGI potential map with an accuracy of 6 mm (FOT, panel I) and 3 mm (L1 norm, panel J). The errors of localization of her anterior lead are 10 mm (FOT, panel K) and 5 mm (L1 norm, panel L), respectively. Evaluation of L2 and L1 norm-based regularization schemes with respect to localization of pacing sites are performed in two more pediatric subjects with epicardial pacing leads : a 16 year old male with tricuspid atresia and L-looped ventricles (s/p Fontan) and a 12 year old female with a single double inlet left ventricle (s/p Fontan). The accuracy of the L1 norm scheme is 3.8±1.5 mm, compared to 9.2±2.6 mm(L2-FOT) and 10±2.8 mm(L2-ZOT).

Pediatric Patient with Wolf-Parkinson-White Syndrome

Figure 7 shows the left lateral view of ECGI activation map in a 5 year old male patient diagnosed with WPW syndrome, with the body-surface ECG delta-wave and QRS morphologies suggesting a left anterolateral or lateral insertion of the accessory pathway. ECGI activation isochrones are displayed in steps of 3 ms for maximum resolution. The FOT reconstructed activation-map shows a large area of early activation (light pink, panel A) around the mitral annulus (MA), confirming a left-sided pathway. With the L1-norm scheme however, two distinct areas of early activation are observed (white, panel B), one in the left lateral (LL) and the other in the left posterolateral (LPL) region near MA, suggesting the presence of two left-sided pathways. This was later confirmed by electrophysiologic study (EPS) and subsequent radiofrequency ablation at two sites, located at 3 o clock (LL) and 5 o clock (LPL) positions around MA, leading to loss of pre-excitation and restoration of normal sinus rhythm.

DISCUSSION

A non-quadratic regularization scheme, constraining the L1-norm of the normal derivative of the solution, was applied to the epicardial potential based inverse problem of electrocardiography. The solution obtained by this new scheme was compared to standard L2-

norm Tikhonov regularization (ZOT and FOT) for experiments with isolated canine hearts, where measured epicardial data were used as the gold standard. Since ZOT does not impose constraints on the gradient but only on the amplitude of the solution, the errors in ZOT originated from incorrect estimation of solution gradients. Consistent with results from previous studies[22,33], FOT which imposed constraint on the solution gradient, had greater accuracy (lower RE) compared to ZOT. However, use of L2-norm in FOT caused spatial smoothing of the solution, which also led to smoother temporal features. This is demonstrated by the infarct substrate data where the L2-norm based regularization failed to accurately reconstruct the multiple deflections in the electrograms from the infarcted area (bottom panels, rows 1 and 2, Figure 4). The L1 norm –based regularization scheme correctly preserved the spatial voltage gradients in the solution, leading to accurate reconstruction of spatiotemporal characteristics of ECGI data. However, for epicardial QRST integral maps (Figure 5), both FOT and L1 norm scheme produced maps with similar accuracy. QRST maps involve a smoothing operation (integration) over the QRST segments of the cardiac cycle, and do not benefit from the "non-smoothing" property of L1 regularization.

The smoothing effect of the L2-norm penalty function was also apparent in the data from pediatric CRT patients where the smaller torso-size of the patient permitted use of only 160–192 body-surface electrodes instead of 250 applied in adult patients. The use of a smaller number of measurement points in conjunction with application of a L2-norm penalty function resulted in overly smoothed solutions and reduced localization capability in smaller two-ventricles and univentricular hearts, as reflected by the ECGI epicardial potential maps during paced rhythms (Figure 6). The L1 regularization scheme led to an improvement in the localization of the pacing sites. Lastly, the single example of the pediatric WPW patient with two left-sided pathways demonstrated the potential clinical benefit of this new regularization scheme. While the Tikhonov regularization showed one large spatially smooth area of early activation, the L1 norm scheme localized two distinct sites of pre-excitation, located laterally and postero-laterally around the left annulus (Figure 7). In general, the L1-norm scheme produced more accurate and higher resolution ECGI maps compared to the standard L2-norm Tikhonov methods.

Computing Time

L1-norm based regularization technique is computationally more complex than L2, due to the non-linearity of the problem. Table 1 compares the computing times (total time for computing potentials over the entire cardiac cycle). By choosing the fixed iterative solution at the (j-1)-th time-step of the cardiac cycle as the initial guess at the j-th time-step, the computing time decreases considerably (~ 5–6 times) compared to the time with an initial guess set to zero at each time-step, without any compromise in solution accuracy. The reduced computing time (< 3 minutes) thus obtained makes this method suitable for clinical application of ECGI.

Acknowledgments

The study was supported by Merit Award R37-HL-33343 and Grant R01-HL-49054 from the National Heart, Lung, and Blood Institute to Y.R. Dr. Rudy is the Fred Saigh Distinguished Professor at Washington University in St. Louis. Y. R. chairs the scientific advisory board and holds equity in CardioInsight Technologies (CIT). CIT does not support any research conducted by Y.R., including that presented here.

References

1. Ahmad GF, Brooks DH, MacLeod RS. An admissible solution approach to inverse electrocardiography. Ann Biomed Eng 1998;26:278–292. [PubMed: 9525768]
2. Bai X V, Towle L, He EJ, He B. Evaluation of cortical current density imaging methods using intracranial electrocorticograms and functional MRI. Neuroimage 2007;35:598–608. [PubMed: 17303438]

3. Barr RC, Spach MS. Inverse calculation of QRS-T epicardial potentials from body surface potential distributions for normal and ectopic beats in the intact dog. Circ Res 1978;42(5):661–675. [PubMed: 76518]
4. Brebbia, CA.; Telles, JCF.; Wrobel, LC. Boundary Element Techniques : Theory and Applications in Engineering. Vol. Ch 2. Berlin: Springer-Verlag; 1984. p. 64-70.
5. Burnes JE, Taccardi B, Ershler P, Rudy Y. Noninvasive electrocardiographic imaging of substrate and intramural ventricular tachycardia in infarcted hearts. J Am Coll Cardiol 2001;38:2071–2078. [PubMed: 11738317]
6. Burnes JE, Taccardi B, MacLeod RS, Rudy Y. Noninvasive ECG imaging of electrophysiologically abnormal substrate in infarcted hearts: A Model Study. Circulation 2000;101:533–540. [PubMed: 10662751]
7. Cheng LK, Bodley JM, Pullan AJ. Comparison of potential- and activation-based formulations for the inverse problem of electrocardiology. IEEE Trans Biomed Eng 2003;50:11–22. [PubMed: 12617520]
8. Colli-Franzone P, Taccardi B, Viganotti C. An approach to inverse calculation of epicardial potentials from body surface maps. Adv Cardiol 1978;21:50–54. [PubMed: 619568]
9. Cuppen J, van Oosterom A. Model studies with the inversely calculated isochrones of ventricular depolarization. IEEE Trans Biomed Eng 1984;BME-31:652–659. [PubMed: 6490025]
10. Ding L, He B. Sparse source imaging in electroencephalography with accurate field modeling. Human Brain Mapping 2008;29:1053–1067. [PubMed: 17894400]
11. Dobson DC, Santosa F. Recovery of blocky images from noisy and blurred data. SIAM J App Math 1996;56:1181–1198.
12. Fischer G, Tilg B, Wach P, Modre R, Leder U, Nowak H. Application of high-order boundary elements to the electrocardiographic inverse problem. Comput Meth Programs Biomed 1999;58:119–131.
13. Geselowitz DB, Miller WT III. A bidomain model for anisotropic cardiac muscle. Ann Biomed Eng 1983;11:191–206. [PubMed: 6670784]
14. Ghanem RN, Burnes JE, Waldo AL, Rudy Y. Imaging dispersion of myocardial repolarization II. Noninvasive reconstruction of epicardial measures. Circulation 2001;104:1306–1312. [PubMed: 11551884]
15. Ghosh S, Rhee EK, Avari JN, Woodard PK, Rudy Y. Cardiac memory in patients with Wolff-Parkinson-White syndrome : noninvasive imaging of activation and repolarization before and after catheter ablation. Circulation 2008;118:907–915. [PubMed: 18697818]
16. Ghosh S, Avari JN, Rhee EK, Woodard PK, Rudy Y. Noninvasive electrocardiographic imaging of epicardial activation before and after catheter ablation of the accessory pathway in a patient with Ebstein anomaly. Heart Rhythm 2008;5:857–860. [PubMed: 18482872]
17. Greensite F, Huiskamp G. An improved method for estimating epicardial potentials from the body surface. IEEE Trans Biomed Eng 1998;45:98–104. [PubMed: 9444844]
18. Hansen PC. The use of L-curve in regularization of ill-posed problems. SIAM J Sci Comput 1993;14:1487–1503.
19. Intini A, Goldstein RN, Jia P, Ramanathan C, Ryu K, Giannattasio B, Gilkeson R, Stambler BS, Brugada P, Stevenson WG, Rudy Y, Waldo AL. Electrocardiographic Imaging (ECGI), a novel diagnostic modality used for mapping of focal left ventricular tachycardia in a young athlete. Heart Rhythm 2005;2:1250–1252. [PubMed: 16253916]
20. Jia P, Ramanathan C, Ghanem RN, Ryu K, Varma N, Rudy Y. Electrocardiographic imaging of cardiac resynchronization therapy in heart failure: observation of variable electrophysiologic responses. Heart Rhythm 2006;3:296–310. [PubMed: 16500302]
21. Karl, WC. Handbook of image and video processing. Bovik, A., editor. Academic Press; San Diego: 2000.
22. Khoury, DS. Use of current density in regularization of the inverse problem of electrocardiography. Proc 16th Intl Conf IEEE EMBS; Baltimore, MD. 1994. p. 133-134.
23. Martin RO, Pilkington TC. Unconstrained inverse electrocardiography :Epicardial potentials. IEEE Trans Biomed Eng 1972;BME-19:276–285. [PubMed: 5036139]
24. Messinger-Rapport BJ, Rudy Y. Non-invasive recovery of epicardial potentials in a realistic heart-torso geometry: normal sinus rhythm. Circ Res 1990;66:1023–1039. [PubMed: 2317885]

25. Messnarz B, Tilg B, Modre R, Fischer G, Hanser F. A new spatiotemporal approach for reconstruction of cardiac transmembrane potential patterns. IEEE Trans Biomed Eng 2004;51:273–281. [PubMed: 14765700]
26. Oster HS, Taccardi B, Lux RL, Ershler PR, Rudy Y. Noninvasive electrocardiographic imaging: Reconstruction of epicardial potentials, electrograms and isochrones, and localization of single and multiple electrocardiac events. Circulation 1997;96:1012–1024. [PubMed: 9264513]
27. Ramanathan C, Ghanem RN, Jia P, Ryu K, Rudy Y. Electrocardiographic imaging (ECGI) : A noninvasive imaging modality for cardiac electrophysiology and arrhythmia. Nat Med 2004;10:422–428. [PubMed: 15034569]
28. Ramanathan C, Jia P, Ghanem RN, Ryu K, Rudy Y. Activation and repolarization of the normal human heart under complete physiological conditions. Proc Nat Acad Sci U S A 2006;103:6309–6314.
29. Rudy Y, Messinger-Rapport BJ. The inverse problem in electrocardiography: solution in terms of epicardial potentials. CRC Crit Rev Biomed Eng 1998;16:215–268.
30. Spach MS, Barr RC. Ventricular intramural and epicardial potential distributions during ventricular activation and repolarization in the intact dog. Circ Res 1975;37:243–257. [PubMed: 1149199]
31. Tikhonov, AN.; Arsenin, VY. Solutions of Ill-posed Problems. New York: Wiley; 1977.
32. Tilg B, Fischer G, Modre R, Hanser F, Messnarz B, Schocke M, Kremser C, Berger T, Hintringer F, Roithinger FX. Model-based imaging of cardiac electrical excitation in humans. IEEE Trans Medical Imaging 2002;21:1031–1039.
33. Throne RD, Olson LG. A comparison of spatial regularization with zero and first order Tikhonov regularization for the inverse problem of electrocardiography. Comput Cardiol 2000;27:493–496.
34. Vogel CR. A fast, robust algorithm for total variation based reconstruction of noisy blurred images. IEEE Trans Image Processing 1998;7:813–824.
35. Wang Y, Cuculich PS, Woodard PK, Lindsay BD, Rudy Y. Focal atrial tachycardia after pulmonary vein isolation : noninvasive mapping with electrocardiographic imaging (ECGI). Heart Rhythm 2007;4:1081–1084. [PubMed: 17675084]
36. Wang Y, Schuessler RB, Damiano RJ, Woodard PK, Rudy Y. Noninvasive electrocardiographic imaging (ECGI) of scar-related atypical atrial flutter. Heart Rhythm 2007;4:1565–1567. [PubMed: 17996498]
37. Wolters, CH.; Anwander, A.; Maess, B.; MacLeod, RS.; Friederici, AD. The influence of volume conduction effects on the EEG/MEG reconstruction of the sources of the early left anterior negativity. Proc. 26th Ann. Intl. Conf. IEEE EMBS; San Francisco, CA, U.S.A. 2004. p. 3569-3572.
38. Zhang X, Ramachandra I, Liu Z, Muneer B, Pogwizd SM, He B. Noninvasive three-dimensional electrocardiographic imaging of ventricular activation sequence. Am J Physiol Heart Circ Physiol 2005;289:2724–2732.

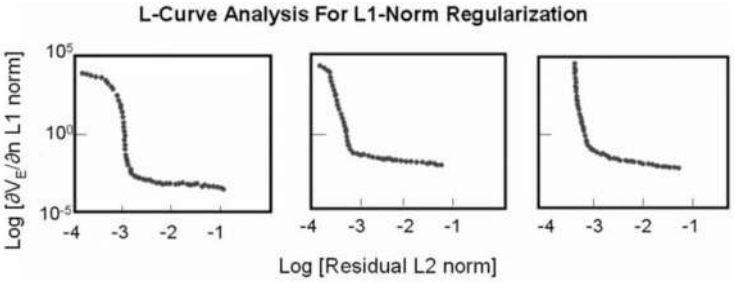

Figure 1.

Logarithmic plots (base 10) of L-curve used for choosing a regularization parameter. The plots are shown for three different datasets : single site pacing in isolated canine heart (left), post-infarct canine data (middle) and WPW patient (right).

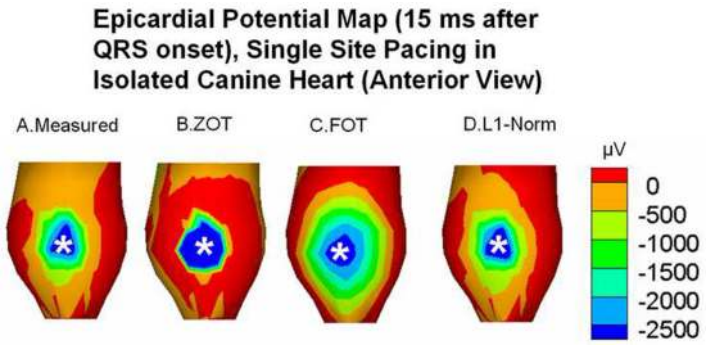

Figure 2.

Epicardial potential map, 15 ms after onset of QRS, comparing measured data (panel A) and reconstructed potentials using zero-order Tikhonov (ZOT, panel B), first order Tikhonov (FOT, panel C) and L1-norm based regularization (panel D) schemes. Asterisk shows the pacing site.

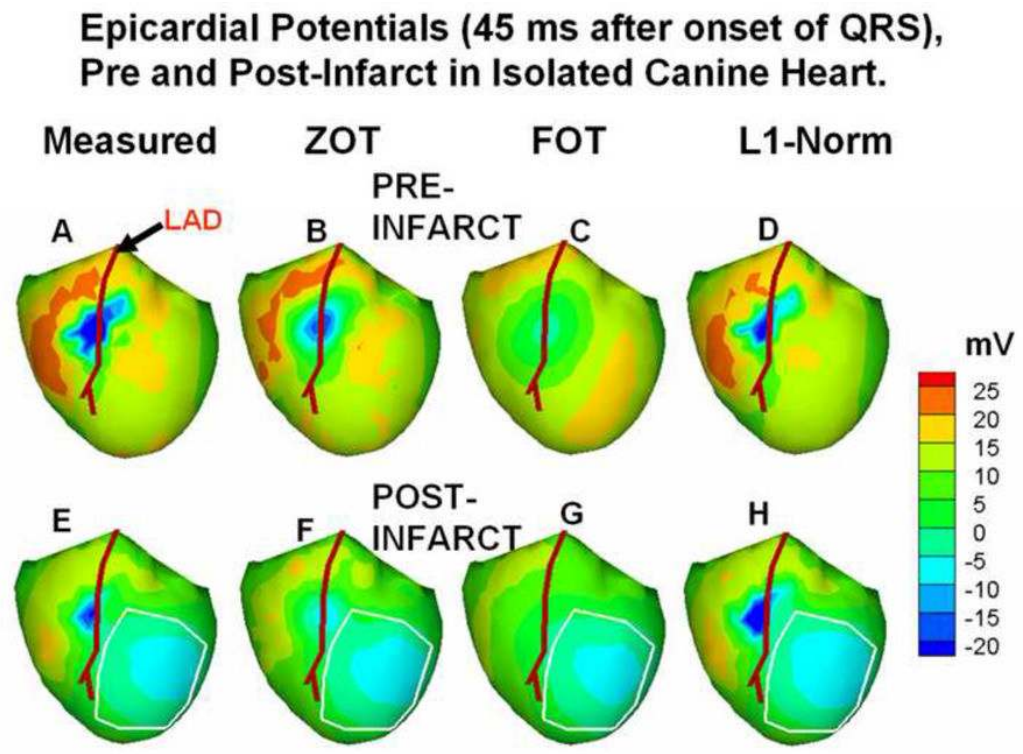

Figure 3.

Epicardial potential maps, 45 ms after onset of QRS, before (top row) and after (bottom) infarct. Measured potentials and reconstructed potentials by ZOT, FOT and L1 norm-based regularization schemes are shown in panels A,B,C,D before infarct and panels E,F,G,H after infarct, respectively. The area of the left ventricular infarct is marked in the panels in the bottom row. The left anterior descending coronary artery (LAD) is shown as an anatomic marker.

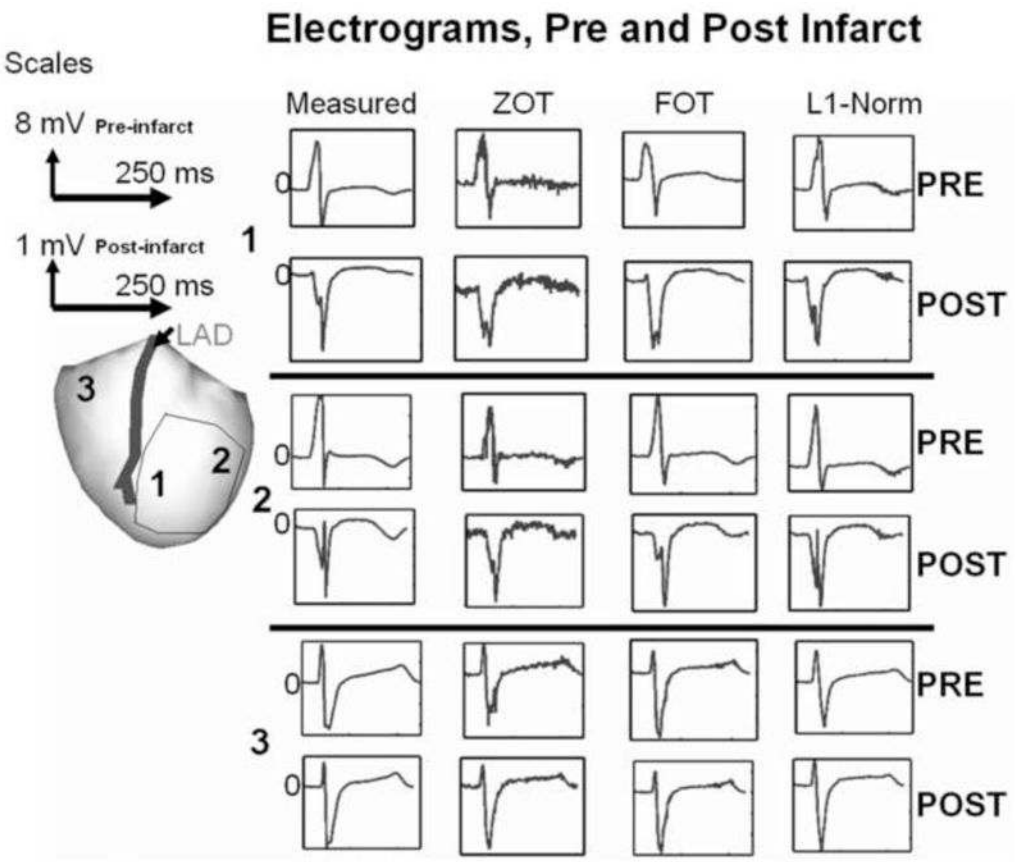

Figure 4.

Measured and reconstructed electrograms by ZOT, FOT and L1-norm based regularization from three different epicardial sites 1,2 and 3. Sites 1 and 2 are within the left ventricular infarct area marked in the cartoon of the heart (left); site 3 is remote to the infarct area. Each panel shows the electrograms pre- (top row) and post-infarct (bottom row) at the corresponding site. Scales are shown in upper left; for site 3 post-infarct scale is the same as pre-infarct scale.

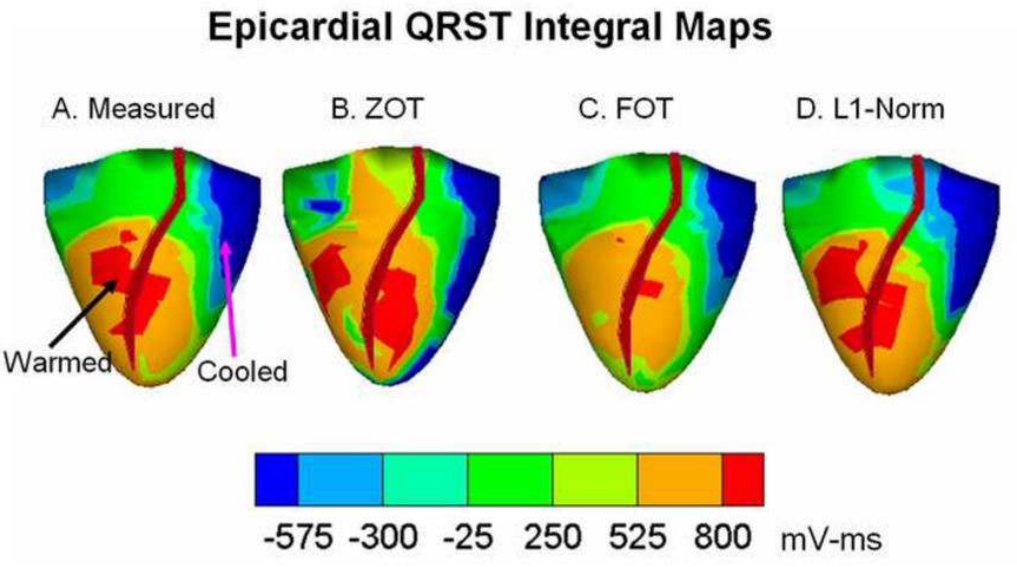

Figure 5.

Epicardial QRST integral maps during simultaneous cooling and warming of adjacent areas on the LV epicardium. Measured QRST integral data are shown in panel A, reconstructed data are shown in panels B (ZOT), C (FOT) and D (L1). The warmed areas have high QRST integral values (red-orange)while the cooled areas have low values (dark blue).

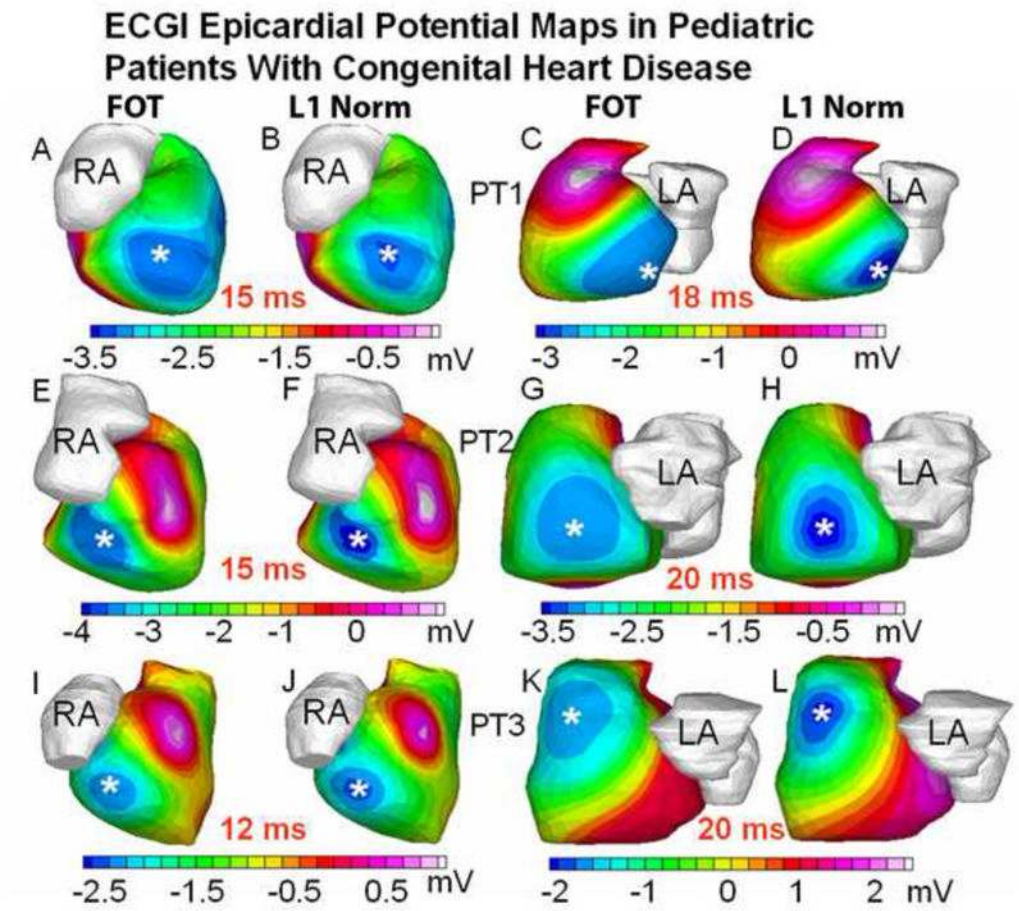

Figure 6.

ECGI epicardial potential maps reconstructed by FOT and L1 regularization, during pacing in pediatric patients with congenital heart disease. Panels A-B, E-F, I-J show the right anterior oblique (RAO) view of the potential map during pacing from the right-sided postero-apical lead in patients PT1, PT2 and PT3 respectively. Panels C-D, G-H and K-L show the epicardial potential maps during pacing from the left-sided lateral leads in the same patients. The tip of the pacing lead is marked by asterisk in each case. The timings (with respect to ECG QRS onset) at which the maps are displayed, are shown in red.

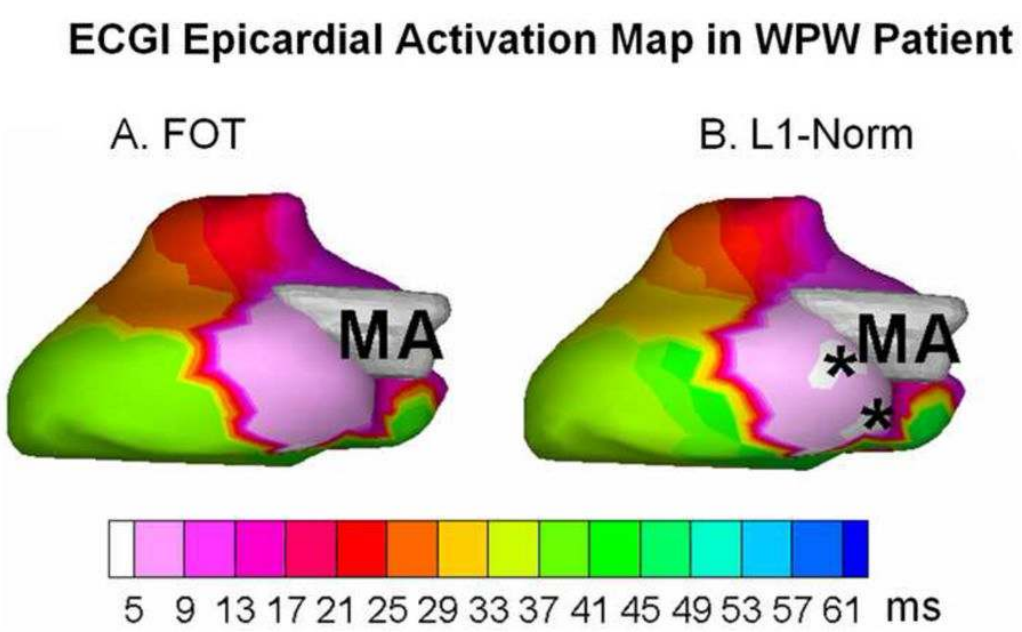

Figure 7.
ECGI activation map (left lateral view) in a pediatric Wolff-Parkinson-White (WPW) patient. Activation maps generated using FOT and L1-norm regularization are shown in panels A and B, respectively. L1-norm activation map shows two discrete areas of early activation (white and black asterisks, panel B) indicating the presence of two left-sided pathways. The FOT map shows one broad area of early activation (light pink, panel A). MA-mitral annulus.

TABLE 1

Computing times (total time for computing epicardial potential maps over the entire cardiac cycle. (ZOT-Zero order Tikhonov, FOT-First order Tikhonov)

Data	ZOT	FOT	L1-norm fixed iterative solution	
			Initial guess zero at every time- step	Initial guess set to solution at previous time-step
Torso-tank	50 s	55 s	6 min 30 s	1 min 45 s
Infarct-Substrate	1 min 30 s	1 min 41 s	10 min 21 s	2 min 38 s
Dispersion of repolarization	30 s	38 s	6 min 4 s	1 min 21 s
Pediatric CRT	1 min 35 s	1 min 41 s	11 min	2 min 50 s
WPW Patient	1 min 44 s	1 min 52 s	11 min 35 s	2 min 55 s

Note: All computing times are measured with respect to a single 3.2 GHz processor with 2 GB memory